BIOCHEMISTRY
including biophysical chemistry & molecular biology

Article

pubs.acs.org/biochemistry

The DNA-Binding Domain of Yeast Rap1 Interacts with Double-Stranded DNA in Multiple Binding Modes

Erik A. Feldmann† and Roberto Galletto*

Department of Biochemistry and Molecular Biophysics, Washington University School of Medicine, St. Louis, Missouri 63110, United States

Supporting Information

ABSTRACT: *Saccharomyces cerevisiae* repressor-activator protein 1 (Rap1) is an essential protein involved in multiple steps of DNA regulation, as an activator in transcription, as a repressor at silencer elements, and as a major component of the shelterin-like complex at telomeres. All the known functions of Rap1 require the known high-affinity and specific interaction of the DNA-binding domain with its recognition sequences. In this work, we focus on the interaction of the DNA-binding domain of Rap1 ($Rap1^{DBD}$) with double-stranded DNA substrates. Unexpectedly, we found that while $Rap1^{DBD}$ forms a high-affinity 1:1 complex with its DNA recognition site, it can also form lower-affinity complexes with higher stoichiometries on DNA. These lower-affinity interactions are independent of the presence of the recognition sequence, and we propose they originate from the ability of $Rap1^{DBD}$ to bind to DNA in two different binding modes. In one high-affinity binding mode, $Rap1^{DBD}$ likely binds in the conformation observed in the available crystal structures. In the other alternative lower-affinity binding mode, we propose that a single Myb-like domain of the $Rap1^{DBD}$ makes interactions with DNA, allowing for more than one protein molecule to bind to the DNA substrates. Our findings suggest that the $Rap1^{DBD}$ does not simply target the protein to its recognition sequence but rather it might be a possible point of regulation.

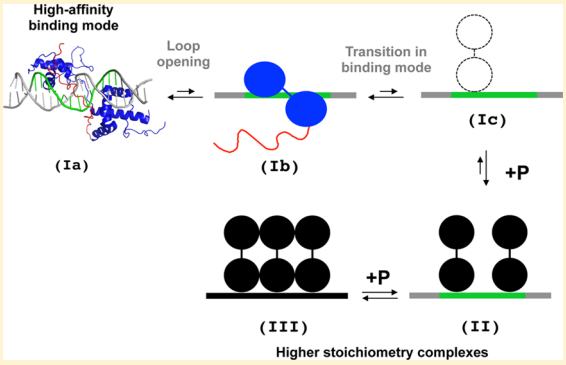

Repressor-activator protein 1 (Rap1) from budding yeast *Saccharomyces cerevisiae* is an essential regulator of transcription and telomere integrity.[1] Rap1 was first identified as a gene repressor at *HML* and *HMR* silent mating-type loci in a process termed gene silencing.[2] Remarkably, Rap1 also acts as an activator of transcription for many glycolytic enzymes and ribosomal proteins, and it has been proposed to bind to ∼5% of genes in yeast accounting for ∼40% of total downstream mRNA transcripts.[3] Rap1 also interacts directly with the Taf4, Taf5, and Taf12 subunits of TFIID, leading to Rap1-controlled transcription of ribosomal protein genes.[4−6] In fact, transcription of ∼50% of RNA polymerase II genes is devoted to ribosomal proteins (RP), and Rap1 is estimated to bind ∼90% of yeast RP promoters.[3,7,8] Rap1 also facilitates recruitment of Fhl1 and Ifh1 to RP gene promoters and in addition recruits a Gcr1−Gcr2 complex to regulate glycolytic enzyme genes.[3,9−11] At telomeres, Rap1 is involved in telomere-length homeostasis through a combination of inhibiting telomere end resection, protecting chromosome ends from telomere fusion, and locally inhibiting the DNA damage response.[12] Rap1 is recruited to the highly repetitive TG-rich DNA repeats of telomeres where it forms the core of the shelterin-like complex together with the Rap1-interacting factors, Rif1 and Rif2.[13−15] It has been proposed that the cell responds to the number of telomeric Rap1−Rif complexes in a mechanism termed "counting" as a method of monitoring the proper elongation of telomeres through inhibition of telomerase.[16,17] Furthermore, Rap1 also interacts with the silencing proteins Sir3 and Sir4, proteins required for telomere positioning and integrity, thus also linking Rap1 to the establishment of the telomere position effect (TPE).[18−20]

Genetic and biochemical studies show that Rap1 has a modular domain organization[21] (Figure 1a). Deletion of the N-terminal region containing a single BRCT domain does not have evident phenotypes.[22] Also, it has been shown that this region does not display any detectable interaction with the rest of the protein[23] but is required for interaction with Gcr1;[24] however, the precise role of the BRCT is still not fully understood. Intriguingly, overexpression of Rap1 is toxic, and part of this putative "Tox" domain comprises residues 598−616, overlapping with the C-terminus of the DNA-binding domain.[25] Deletion of the Tox domain *in vivo* rescues the toxic phenotype upon overexpression.[25] The DNA-binding domain (DBD) of yeast Rap1 is centrally positioned within the full-length protein sequence, spanning residues 358−601 based on electron density provided from the most recent crystal structure of the DBD−DNA complex.[23] The region comprising residues 591−597, the end of the C-terminal tail of the DNA-binding domain, appears to be important for viability, although it does

Received: August 20, 2014
Revised: November 6, 2014
Published: November 9, 2014

dx.doi.org/10.1021/bi501049b | *Biochemistry* 2014, 53, 7471−7483

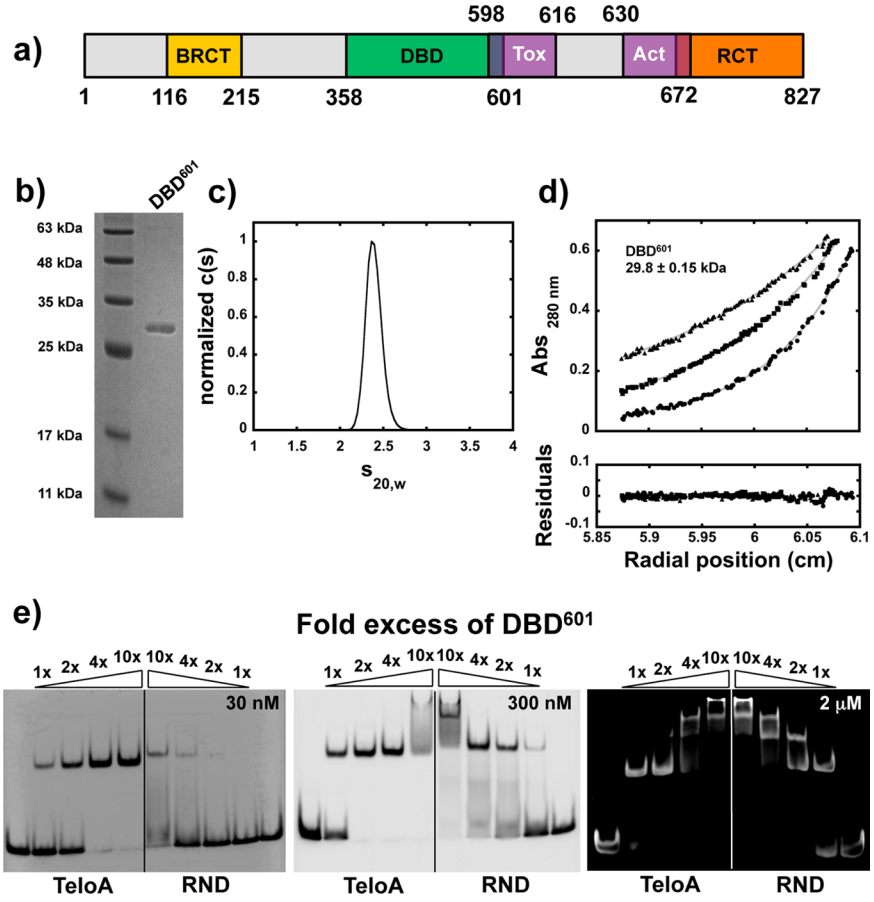

Figure 1. Monomers of DBD^{601} bind DNA with a higher than expected stoichiometry. (a) Modular organization of the full-length Rap1 protein sequence with selected domains highlighted: BRCT, BRCA1 C-terminal domain; DBD, DNA-binding domain; Tox, toxicity region; Act, activation region; RCT, Rap1 C-terminal domain. (b) Sodium dodecyl sulfate−polyacrylamide gel electrophoresis of purified DBD^{601} stained with Coomassie Blue. (c) Distribution of sedimentation coefficients for 20 μM DBD^{601} in buffer HN_{50} showing a single species of 2.4 S. (d) Sedimentation equilibrium profiles of 20 μM DBD^{601} in buffer HN_{50} at rotor speeds of 16000, 20000, and 24000 rpm. The solid gray lines are the global analyses of the data fit with a single-species model with an observed M_w of 29.8 kDa, consistent with the M_w of a monomer. (e) Gel electrophoretic mobility shift assays performed at the indicated excesses of DBD^{601} with either 30 nM (left) or 300 nM (middle) TeloA and RND labeled at the 5′-end of the top strand with FAM. The right panel shows an EMSA performed at 2 μM unlabeled TeloA and RND, stained postelectrophoresis.

not dramatically affect DNA binding.[23] Finally, the C-terminal region of the protein (RCT) is where most of the functional interactions are believed to occur,[15,18,26,27] yet little is known of the linkage between Rap1 DNA binding and interaction of the RCT with interacting factors.

When bound to double-stranded DNA (dsDNA) containing a Rap1 recognition sequence, the Rap1^{DBD} structure adopts two Myb-type α-helical bundles separated by a disordered linker region and flanked by the unstructured C-terminal tail.[28] From available crystal structures of various Rap1^{DBD}−DNA complexes, it has been shown that the DBD orients in such a way that both Myb motifs and the C-terminal tail make contact with the DNA double helix interacting directly with nucleotide bases and the phosphate backbone.[29] This structural arrangement is preserved on complexes containing either telomeric or nontelomeric recognition sequences. A typical Rap1 recognition sequence is composed of a 13 bp sequence with two 5 bp hemisites separated by a 3 bp spacer.[30,31] Interestingly, previous work has shown that Rap1 can also bind with a lower affinity to a single hemisite.[32]

All the activities of Rap1 appear to occur through its DNA-bound state, and the available data provide a model for binding of Rap1 to DNA with high affinity, in a simple 1:1 complex with its recognition site.[4,23,29,33] The current molecular picture of how Rap1 interacts with its recognition sequences is largely based on the available crystal structures of the DNA-binding domain,[23,28,29] and this provides a great model for understanding the role of this essential domain of the protein. In this study, we examined the interaction with model DNA substrates of a Rap1^{DBD} construct that comprises residues 358−601 (DBD^{601}) observed in the most recent crystal structure.[23] Unexpectedly, we found that this DBD^{601} construct, in addition to forming a 1:1 high-affinity complex, can form complexes with higher than anticipated stoichiometries. We propose that the Rap1^{DBD} is able to bind dsDNA minimally in two binding modes. In one mode, both Myb-like domains bind to the recognition sequence as shown in the crystal structures;[23,28,29] in the alternative lower-affinity mode, only one Myb-like domain binds to the DNA.

MATERIALS AND METHODS

Reagents and Buffers. All chemicals used were reagent grade. All solutions were prepared with distilled and deionized Milli-Q water (18 MΩ at 25 °C). All oligonucleotides were purchased from Integrated DNA Technologies (IDT, Coralville, IA). The oligonucleotides used for cloning purposes were

dx.doi.org/10.1021/bi501049b | Biochemistry 2014, 53, 7471−7483

purified by standard desalting, whereas oligonucleotides used for binding experiments were all purified via high-performance liquid chromatography, suspended in TE buffer [10 mM Tris-HCl (pH 8.3) and 0.1 mM EDTA]; the concentration was determined spectrophotometrically using the extinction coefficients provided. The sequence composition of the "top" strand of the oligonucleotides used is shown in Table 1, and the position of the FAM or Cy3 fluorescent labels is indicated in the text. All annealed duplex dsDNAs were prepared by mixing equimolar concentrations of each oligonucleotide strand in 20 mM (HEPES) (pH 7.4), 50 mM NaCl, 10% (v/v) glycerol, and 2 mM $MgCl_2$ and incubated in a preheated 95 °C water bath, followed by slow cooling to room temperature.

Table 1. Sequences of the dsDNA Substrates Used in This Work

	Rap1 recognition sequence is bolded on the "top" strand	Modifications
TeloA	5′-CCGC**ACACCCACACACC**AGTG GGCGTGTGGGTGTGTGGTCAC	Top: 5′-FAM or Cy3, 3′-FAM Bott: 5′-FAM, 3′-FAM
RPG	5′-CCGC**ACACCCATACATT**AGTG GGCGTGTGGGTATGTAATCAC	Top: 5′-FAM or Cy3
HMRE	5′-CCGC**AA**ACCC**ATCAA**CCAGTG GGCGTTTGGGTAGTTGGTGAC	Top: 5′-FAM or Cy3, 3′-FAM
RND	5′-CCGCCGCGGAACTTATTAGTG GGCGGCGCCTTGAATAATCAC	Top: 5′-FAM or Cy3, 3′-FAM

Cloning, Overexpression, and Purification of Rap1 Constructs. Full-length Rap1 was initially cloned from *S. cerevisiae* strain W303 and provided in pET30a (Recombinant DNA Laboratory, University of Texas Medical Branch, Galveston, TX). The gene encoding Rap1 (residues 1−827) was recloned into pGEX-6p-1 with a PreScission HRV 3C-cleavable N-terminal GST tag. This plasmid was used as a template to amplify the DNA-binding domain of Rap1 (residues 358−601, DBD^{601}), which was subsequently cloned into pGEX-6p-1 at EcoRI and XhoI restriction sites, leaving six amino acids after digestion with 3C protease. The resulting plasmid was transformed into *Escherichia coli* Rosetta2(DE3)-pLysS cells (EMD Chemicals, Novagen, Gibbstown, NJ) for overexpression in LB-Miller broth. Cells were allowed to grow at 37 °C until the OD_{600} measured 0.6−0.8, quickly chilled, and induced with 0.7 mM IPTG at 16 °C for overnight expression. Harvested cell pellets were stored at −80 °C for later use.

Cell pellets were thawed on ice, suspended at a density of 20 mL/g of cell paste in lysis buffer [20 mM sodium phosphate (pH 7.3), 400 mM NaCl, 10% (v/v) glycerol, 1 mM DTT, 0.5 mM EDTA, and 0.1 mM phenylmethanesulfonyl fluoride (PMSF)], lysed by sonication, and centrifuged at 25000*g* for 60 min at 4 °C. Clarified cell lysates were incubated with 0.3% (v/v) polyethylenimine while being gently stirred at 4 °C followed by centrifugation at 25000*g* for 60 min. The resulting clarified supernatant was diluted 2-fold in lysis buffer and then incubated with Glutathione Sepharose 4 Fast Flow GST-affinity resin (GE Healthcare Bio Sciences, Piscataway, NJ) for overnight binding at 4 °C with gentle stirring. Unbound proteins were removed by first washing with lysis buffer, followed by a high-salt wash of lysis buffer spiked to 1 M NaCl, and then finally equilibrated with buffer D [20 mM Tris-HCl (pH 8.3 at 4 °C), 150 mM NaCl, 10% (v/v) glycerol, 1 mM DTT, 0.5 mM EDTA, and 0.1 mM PMSF]. The glutathione resin was then suspended in 10 column volumes of buffer D and incubated with PreScission HRV-3C protease (kind gift of P. M. Burgers) overnight at 4 °C with gentle stirring. Cleaved DBD^{601} was collected as the flow-through fraction and then loaded on a Poros 50 HE Heparin column (Life Technologies, Applied Biosystems, Foster City, CA) equilibrated with buffer D, followed by washing with buffer D containing 300 mM NaCl and then elution in buffer D containing 600 mM NaCl. Purified DBD^{601} was dialyzed against storage buffer [20 mM HEPES (pH 7.4), 400 mM NaCl, 40% (v/v) glycerol, 1 mM DTT, and 0.5 mM EDTA] and then stored at −80 °C. Before the experiments, DBD^{601} was dialyzed against buffer HN_{50} [20 mM HEPES (pH 7.4), 50 mM NaCl, 2 mM $MgCl_2$, and 10% (v/v) glycerol] and the concentration determined using an extinction coefficient of 24870 M^{-1} cm^{-1}.[60,61]

Analytical Ultracentrifugation. All sedimentation experiments were conducted on an Optima XL-A analytical ultracentrifuge using an An60Ti rotor (Beckman Coulter, Brea, CA). Sedimentation velocity experiments were performed using Epon charcoal-filled double-sector centerpieces at 55000 rpm with 0.03 cm spacing and recording scans every 8 min. For sedimentation velocity experiments with DBD^{601} alone, absorbance scans were recorded at 280 nm, whereas in experiments with Cy3-labeled DNA, scans were recorded at 545 nm where protein does not contribute to the signal. Velocity profiles were processed and analyzed with SedFit (P. Schuck, National Institute of Biomedical Imaging and Bioengineering, National Institutes of Health, Bethesda, MD),[34−37] and the apparent sedimentation coefficient was corrected for temperature and buffer composition using SEDNTERP.[38]

Sedimentation equilibrium experiments were performed using Epon charcoal-filled six-sector centerpieces at the appropriate revolutions per minute with 0.001 cm spacing, scanned every 4 h, and averaged from 10 replicates. Equilibrium experiments of DBD^{601} alone were once again conducted at 280 nm and experiments with Cy3-labeled DNA at 545 nm. Achievement of equilibrium was determined by the overlap of scans at 4 h separation and checked with SedFit. Sedimentation equilibrium profiles were processed and analyzed with SedFit/SedPhat (P. Schuck). The apparent molecular weights were determined using the partial specific volume calculated from the amino acid composition of DBD^{601} (0.726 mL/g at 20 °C) and a partial specific volume for DNA of 0.527 mL/g at 20 °C, determined experimentally by fitting for the partial specific volume given the known M_w of the DNA. The partial specific volume of the protein in complex with DNA was calculated from[39]

$$\nu_{PD} = \frac{nM_P\nu_P + M_D\nu_D}{nM_P + M_D}$$

where n is the number of DBD^{601} molecules in the complex, M_P and M_D are the molecular weights of DBD^{601} and the DNA, respectively, ν_P is the partial specific volume of DBD^{601}, and ν_D is the partial specific volume of the labeled DNA.

Equilibrium Fluorescence Titrations. All fluorescence titrations were performed with an L-format PC1 spectrofluorimeter (ISS, Champaign, IL) equipped with Glan-Thompson polarizers. Measurements of the anisotropy and total fluorescence intensity of FAM-labeled dsDNA were

dx.doi.org/10.1021/bi501049b | *Biochemistry* 2014, 53, 7471−7483

recorded using excitation and emission wavelengths of 480 and 530 nm, respectively, using

$$r = \frac{I_{VV} - GI_{VH}}{I_{TOT}}$$

where $I_{TOT} = I_{VV} + 2GI_{VH}$ and G is the G factor.[40] The change in total fluorescence intensity relative to the value of dsDNA only is reported. Titrations were performed with a 1 cm × 1 cm quartz cuvette, stirring for 2 min between additions. The total volume of added protein was maintained within 4−7% of the initial volume and corrected accordingly.[41] All titrations were conducted at 20 °C in buffer HN_{50} or the same buffer but with different NaCl concentrations where indicated. Comparison of four independent DBD^{601} preparations using two separate batches of synthesized oligonucleotides for a reference dsDNA substrate shows that the standard deviation of the measured fluorescence anisotropy is less than 3−5%, smaller than the size point used in the figures.

Electrophoretic Mobility Shift Assays. Samples of FAM-labeled dsDNAs and DBD^{601} were incubated for 10 min at room temperature in buffer HN_{50} and then loaded on 8% acrylamide/bisacrylamide 1× TBE mini gels with running buffer prechilled at 4 °C. Electrophoretic migration was conducted at a constant voltage of 80 V for 70 min at 4 °C. Gels were scanned using a Typhoon 9400 Variable Mode Imager (Amersham BioSciences, GE Healthcare Bio Sciences) after excitation of the fluorophore with the blue laser (488 nm) setting. EMSAs involving unlabeled DNA were subjected to identical incubation and electrophoresis treatments, stained in 1× TBE buffer with GelRed (Phenix Research, Candler, NC) for 15 min, and scanned on an Alpha Imager HP imager (Protein Simple, Santa Clara, CA).

Isothermal Titration Calorimetry. The experiments were performed using a VP-ITC calorimeter (Microcal, GE Healthcare Bio Sciences) after extensive dialysis of both DBD^{601} and the DNA in buffer HN_{50} or HN_{150} (the subscript stands for 150 mM NaCl). Titrations were conducted with 27 injections (10 μL each, 2 μL initial injection) of 20 μM titrant into 2 μM samples containing either DBD^{601} or duplex DNA, at 20 °C with 300 s between injections. Reference titrations to account for the heat of dilution of each titrant were performed by titrating into sample cells loaded with the appropriate reaction buffer and equilibrated at the appropriate temperature.

RESULTS

The DNA-Binding Domain of Rap1 Binds dsDNA with a Higher Than Expected Stoichiometry. We generated a construct of the DNA-binding domain of *S. cerevisiae* Rap1 that comprises residues 358−601 (DBD^{601}) (Figure 1a), as observed in the most recent X-ray crystal structure in complex with DNA.[23] The DBD^{601} was overexpressed and purified as a soluble protein after cleavage of a N-terminal GST fusion tag (Figure 1b). This avoids the need for any refolding steps,[28,29,42] as already shown in previous work.[4] At the maximal DBD^{601} concentrations used in the binding studies (15−20 μM), sedimentation velocity and equilibrium analytical ultracentrifugation show that DBD^{601} is a monomer in solution (Figure 1c,d). The model dsDNA substrates used in this work are 21 bp long and contain a Rap1 recognition sequence flanked by constant 4 bp "handles" (Table 1). Following previous studies of binding of Rap1 to DNA, we designed substrates with three different recognition sequences that are found at telomeres (TeloA),[23,29] ribosomal protein genes (RPG),[1] and silencer elements (HMRE),[1,29] and a control DNA in which the 13 bp recognition sequence was replaced with a random one (RND) (Table 1).

Figure 1e shows a gel electrophoretic mobility shift assay (EMSA) of either a TeloA or a RND dsDNA substrate labeled with 6-carboxyfluorescein (FAM) at the 5′-end of the top strand (Table 1). At a dsDNA concentration of 30 nM, DBD^{601} binds to TeloA but little to RND, consistent with previous reports of high affinity for its recognition sequence.[29] Increasing the DNA concentration should not have any effect other than to populate the 1:1 complex of DBD^{601} for the lower-affinity RND substrate. Indeed, at 300 nM dsDNA, DBD^{601} binds also to the RND substrate (Figure 1e, middle panel). Surprisingly, at these higher DNA concentrations, we also observe the appearance of a supershift for both the TeloA and RND substrates, suggesting that more than one DBD^{601} molecule can bind at saturation. Such a supershift is absent in EMSAs performed at 30 nM with TeloA. This would suggest that on this substrate formation of the higher-stoichiometry complexes of DBD^{601} is weak (see below).

To test whether the appearance of this supershift is simply due to the presence of the fluorescent label at the 5′-end of the substrates, we next performed EMSAs with 2 μM unlabeled TeloA and stained the nucleic acid postelectrophoresis (Figure 1e, right panel). At this higher concentration of TeloA, the formation of supershifted bands becomes evident even at a 4-fold excess of protein over DNA. For the RND substrate, the supershifted bands appear at an even lower DBD^{601} ratio, suggesting that when the recognition sequence is absent it is easier to populate these higher-order complexes. Similar data are also observed with DNA sequences containing either the RPG or HMRE recognition sequence (data not shown).

DBD^{601}−DNA Complexes with High Stoichiometry Are Clearly Observed by Analytical Ultracentrifugation. While the EMSAs show evidence of the formation of higher-order DBD^{601}−DNA complexes, the data also show that at the higher DBD^{601} concentrations there is a distribution of multiply ligated species (Figure 1e, right panel). To test whether this distribution is also present in solution, we performed analytical sedimentation velocity experiments using TeloA labeled at the 5′-end of the top strand with Cy3, monitoring Cy3 absorbance at 545 nm where there is no contribution from protein to the signal. Figure 2a shows the distribution of sedimentation coefficients [$c(s)$] obtained at different DBD^{601} loading concentrations in buffer HN_{50} [20 mM HEPES (pH 7.4), 50 mM NaCl, 2 mM $MgCl_2$, and 10% (v/v) glycerol]. At substoichiometric concentrations of DBD^{601}, the peak corresponding to free dsDNA is clearly observable and, within error, migrates at the same position as free DNA. At stoichiometric concentrations, only a slight population of free TeloA can be observed, while the majority of the DNA is bound in a singly ligated complex with an $s_{20,w}$ of 3.6 S. At a 2:1 DBD^{601}:DNA loading ratio, only subtle changes in the $s_{20,w}$ value are detectable, whereas at a 10-fold excess of DBD^{601}, the DNA-bound species shows a single peak that sediments with a high $s_{20,w}$ value (5.6 S). The molecular weight of this species estimated from the $s_{20,w}$ (∼99.7 kDa; P/D_{calc} ∼ 2.9) suggests that approximately three DBD^{601} molecules bind at saturation. In Figure 2a, we also show the distribution of $c(s)$ obtained for unlabeled TeloA in the presence of an 8-fold excess of DBD^{601} while monitoring the absorbance at 260 nm, where the protein signal is minimal at this DNA concentration. Consistent with

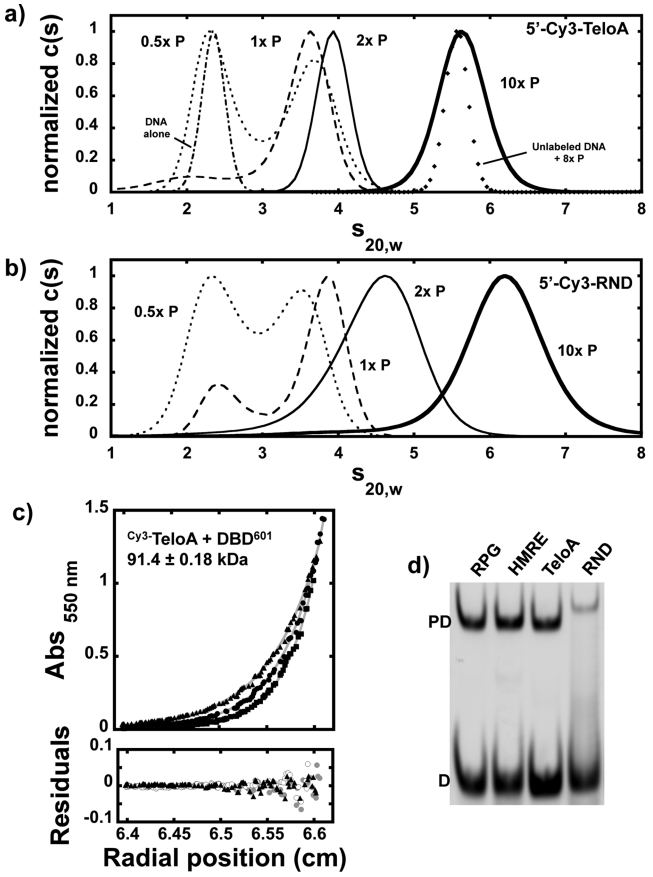

Figure 2. DBD^{601}–DNA complexes of higher strochiometry monitored by analytical ultracentrifugation. (a) Sedimentation coefficient distributions from velocity experiments with 2 μM Cy3-labeled TeloA in buffer HN_{50} at different DBD^{601}:DNA ratios: 0.5 (···), 1 (---), 2 (thin solid line), and 10 (thick solid line). The data for Cy3-labeled TeloA alone are shown, as well. The distribution of sedimentation coefficients with unlabeled TeloA and an 8-fold excess of DBD^{601} is included, as well (diamonds). (b) Same experiments as in panel a but with Cy3-labeled RND. (c) Sedimentation equilibrium profile of 1.5 μM Cy3-labeled TeloA in the presence of an 8-fold excess of DBD^{601} in buffer HN_{50} at rotor speeds of 14000, 16000, and 18000 rpm. The solid gray lines are the global analyses of the data fit with a single-species model (see Table 2). (d) EMSA of protein–DNA complexes formed at a 1:1 ratio with different 21 bp substrates at 300 nM.

the data for Cy3-labeled TeloA, the protein–DNA complex sediments with a high $s_{20,w}$ value (5.55 S). Together with the EMSA in Figure 1e, these data indicate that even if the label were to affect the detailed energetics of the interaction, formation of the larger DBD^{601}–TeloA complexes is label-independent. Finally, the appearance of a single peak in the $c(s)$ distribution observed at this high DBD^{601} loading ratio strongly suggests a relatively homogeneous distribution of bound species. Therefore, the apparent distribution of multiply ligated species that are observed by EMSA most likely results from the dissociation of the higher-stoichiometry complexes during electrophoresis.

Results of identical experiments performed on the 5′-Cy3-labeled RND substrate are shown in Figure 2b. Similar to TeloA, on the RND substrate at a 10-fold excess of DBD^{601}, the $c(s)$ distribution shows a large increase in $s_{20,w}$. Once again, these data show that formation of these larger protein–DNA complexes is independent of the presence of a Rap1 recognition sequence in the substrate. We also note that at substoichiometric protein concentrations, the apparent fraction of the singly ligated species from the $c(s)$ distribution is similar for TeloA and RND. This suggests that some dissociation of the bound DBD^{601} occurs during electrophoresis, especially for the lower-affinity complexes formed on RND (Figure 1e). Interestingly, at a 2-fold excess of DBD^{601} on the RND substrate, the $s_{20,w}$ (4.6 S) is greater than that observed with TeloA (3.9 S), suggesting that on this substrate DBD^{601} might be either more prone to accessing higher-stoichiometry complexes or in a different conformation. Also, at 10-fold excess of protein, the $s_{20,w}$ is larger on RND (6.2 S) than on TeloA (5.6 S) and the molecular weight estimated for this complex (~124.5 kDa, $P/D_{calc} \sim 3.7$) would suggest that more than three DBD^{601} molecules could bind at saturation. However, this is surprising because the length of the DNA is the same for both TeloA and RND substrates and the same maximal stoichiometry might be expected. Alternatively, the observed differences in the $s_{20,w}$ may reflect different conformations and/or large conformational changes of the DBD^{601} complexes formed on these two substrates (see below).

To determine the stoichiometry of the DBD–DNA complexes, we performed analytical sedimentation equilibrium experiments with complexes of Cy3-labeled TeloA or RND substrates formed at a 8-fold loading ratio of DBD^{601} to DNA. Figure 2c shows the equilibrium absorbance profile at three different rotor speeds for Cy3-labeled TeloA (RND data set not shown). Consistent with the presence of a single peak in the $c(s)$ distribution (Figure 2a), a single-species model is sufficient to fit the data (residuals in Figure 2c). The molecular weights determined from global fitting of the three-speed equilibrium data sets for TeloA and RND in complex with an 8-fold excess of DBD^{601} are listed in Table 2. The stoichiometry of the DBD^{601}–DNA complexes calculated from the observed molecular weights is consistent with three DBD^{601} molecules binding to either dsDNA substrate at saturation. This indicates that the larger $s_{20,w}$ observed for the complex formed on the RND substrate (Figure 2b) originates from different con-

Table 2. Molecular Weights of DBD^{601}–DNA Complexes Determined by Equilibrium Analytical Sedimentation at Different NaCl Concentrations

	5′-Cy3-TeloA		5′-Cy3-RND		5′-Cy3-HMRE	
[NaCl] (mM)	Mw_{obs}[a] (kDa)	P/D[b]	Mw_{obs} (kDa)	P/D	Mw_{obs} (kDa)	P/D
50	91.4 ± 0.2	2.61 ± 0.02	93.9 ± 0.2	2.69 ± 0.02	96.1 ± 0.5	2.77 ± 0.03
100	87.8 ± 0.1	2.49 ± 0.02	89.6 ± 0.3	2.55 ± 0.01	90.2 ± 0.1	2.57 ± 0.02
150	57.4 ± 0.1 (68.8 ± 0.3)[c]	1.47 ± 0.02 (1.85 ± 0.02)[c]	68.5 ± 0.3	1.84 ± 0.02	63.8 ± 0.2	1.68 ± 0.02

[a] ν_{P3D} = 0.7 mL/g, w-avg using ν_P = 0.726 mL/g, and ν_D = 0.527 mL/g determined for Cy3-TeloA. [b] Based on Mw_{dsDNA} = 13.6 kDa and Mw_{DBD} = 29.8 ± 0.15 kDa. [c] Determined for a 20-fold molar excess.

dx.doi.org/10.1021/bi501049b | Biochemistry 2014, 53, 7471–7483

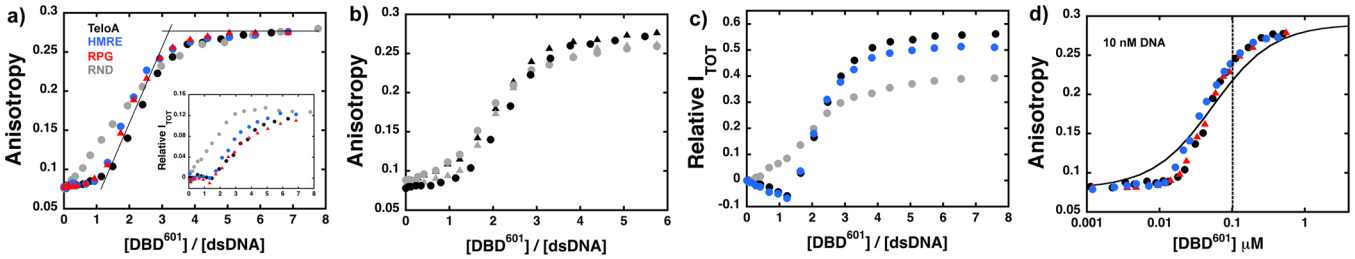

Figure 3. DBD^{601} binding to FAM-labeled dsDNA substrates monitored by fluorescence anisotropy confirms the formation of high-stoichiometry complexes. (a) Change in the fluorescence anisotropy and relative total intensity (inset) of 255 nM dsDNAs labeled at the 5′-end of the top strand in buffer HN_{50} as a function of protein to DNA total concentration ratio for TeloA (black), RND (gray), HMRE (blue), and RPG (red). (b) Change in the fluorescence anisotropy of FAM-labeled TeloA where the fluorophore is positioned at various ends of the dsDNA duplex: circles for the 5′-end (black) or 3′-end (gray) of the top strand and triangles for the 5′-end (black) or 3′-end (gray) of the bottom strand. (c) Change in the relative total intensity in buffer HN_{50} as a function of DBD^{601}:DNA ratio for 255 nM dsDNA labeled with FAM at the 3′-end of the top strand: TeloA (black), RND (gray), and HMRE (blue). (d) Change in the fluorescence anisotropy in buffer HN_{50} as a function of DBD^{601} concentration for 10 nM dsDNA labeled with FAM at the 5′-end of the top strand: TeloA (black), RPG (red), and HMRE (blue).

formations and/or large conformational changes rather than from the ability to bind one additional molecule.

In this regard, we also note that although small, there are differences in the sedimentation coefficient of complexes formed at equimolar concentrations on either TeloA (3.6 S) or RND (3.85 S) (Figure 2a,b), suggesting that even the singly ligated species might be in a different conformation. This is further supported by differences in the electrophoretic mobility of the singly ligated species. Figure 2d shows an EMSA for complexes of DBD^{601} formed at a 1:1 ratio with 300 nM DNAs labeled with FAM at the 5′-end of the top strand. Despite the fact that these substrates are identical in length (21 bp), on RND we observe a slower migrating band, suggesting this complex is different from those formed on either TeloA, RPG, or HMRE, each of which contains a recognition sequence.

Equilibrium Fluorescence Titrations Confirm the Formation of High-Stoichiometry Complexes and Suggest Different Conformations of the Singly Ligated Species. Next we examined the binding of DBD^{601} in solution using fluorescence spectroscopy while monitoring the signals from fluorescently labeled DNA substrates. Figure 3a shows the change in fluorescence anisotropy of 255 nM dsDNA substrates [TeloA, HMRE, RPG, and RND labeled at the 5′-end of the top strand with FAM (see Table 1)] as a function of the ratio of the total protein to DNA concentration in buffer HN_{50} [20 mM HEPES (pH 7.4), 50 mM NaCl, 2 mM $MgCl_2$, and 10% (v/v) glycerol]. Binding of DBD^{601} to these 5′-labeled dsDNAs is accompanied by a large increase in fluorescence anisotropy, providing a large signal change to monitor the reaction. Although tight binding conditions for the higher-stoichiometry complexes cannot be fully achieved, these data strongly suggest that at saturation approximately three DBD^{601} molecules bind to the DNA, regardless of the presence or absence of a Rap1 recognition sequence. This provides further support to the conclusions from analytical ultracentrifugation experiments performed at higher DNA concentrations (Table 2).

We also note the interesting behavior of the fluorescence anisotropy at low protein saturation, where the singly ligated species is populated. While for the RND substrate the fluorescence anisotropy increases linearly, binding of the first DBD^{601} molecule to the dsDNA substrates containing any of the Rap1 recognition sequences is accompanied by a small ~15% change in anisotropy (from 0.078 to ~0.09). This is unexpected given that DBD^{601} clearly binds these dsDNA substrates, and presumably with higher affinity than for RND (Figure 1e). One simple origin of this behavior might be the presence of large changes in the fluorescence quantum yield of the fluorophore that would contribute to distortions of the observed anisotropy.[41,43,44] However, this does not appear to be the case. The inset in Figure 3a shows the change in total fluorescence intensity observed for these substrates. No more than a 10−12% fluorescence increase is observed at saturation. Rather, at low protein saturation, the total fluorescence intensity shows a behavior qualitatively similar to that of fluorescence anisotropy. Independent of the recognition sequence, when a high-affinity site is present in the substrate, the signal is dominated by the binding of the second and third protein molecules. This peculiar dependence of the fluorescence anisotropy at low DBD^{601} saturation is also observed at higher pH, strongly suggesting that this behavior is not due to a possible effect on the quantum yield of the different protonation states of 6-carboxyfluorescein (not shown).[45] Preliminary experiments monitoring the effect of DBD^{601} on the lifetime and fluorescence correlation times of 5′-end FAM-labeled TeloA show no change in either parameter, consistent with the observed lack of anisotropy and fluorescence change (not shown). Moreover, qualitatively similar behavior on TeloA is also observed when monitoring the fluorescence change of Cy3 instead of FAM (not shown). Finally, Figure 3b shows the change in fluorescence anisotropy of TeloA in which the fluorescent label was placed at any of the four end positions of the substrate. Within error, the data show that independent of the position of the fluorophore, binding of the first molecule of DBD^{601} makes a small contribution to the change in anisotropy while the signal is dominated by the binding of the second and third molecules.

Interestingly, when the label is at the 3′-end position of the dsDNAs, binding of DBD^{601} is accompanied by very different changes in fluorescence intensity as compared to the 5′-end position. Figure 3c shows the relative change in total fluorescence intensity at different ratios of total protein to DNA concentration for TeloA, HMRE, and RND substrates with the label placed at the 3′-end of the top strand. In this case, binding of the first molecule of DBD^{601} to either TeloA or HMRE now leads to fluorescence quenching (~7−8%), followed by a large fluorescence increase (~57%) when the second and third molecules bind. However, on the RND substrate, binding of the first molecule leads to an immediate fluorescence increase (~7%), though at saturation the maximal change is smaller than that for TeloA or HMRE. Once again,

dx.doi.org/10.1021/bi501049b | Biochemistry 2014, 53, 7471−7483

even when the fluorescent label is placed at the 3′-end, binding of DBD^{601} to substrates containing the recognition sequence reveals a signal signature different from that of a DNA of random composition. Regardless of the location of the fluorescent label, the data strongly suggest that these signatures in signal for the singly ligated species must be an intrinsic property of the system.

The equilibrium fluorescence experiments were performed at DNA concentrations where by an EMSA a supershift starts to be detected at the higher DBD^{601} concentrations. However, EMSAs with 30 nM TeloA show only a single shifted band even at 10-fold excess of protein, suggesting that at this lower DNA concentration the higher-stoichiometry complexes do not form (i.e., weak). Moreover, the data in Figure 3a show that formation of the 1:1 complex with DNAs containing a Rap1 recognition sequence is accompanied by a small change in anisotropy. Therefore, for experiments performed at <30 nM DNA only a 1:1 complex should be populated, and on these substrates, little change in anisotropy should be detected. This is clearly not the case. Figure 3d shows the change in fluorescence anisotropy of 10 nM TeloA, HMRE, and RPG (labeled at the 5′-end of the top strand with FAM) as a function of DBD^{601} concentration in buffer HN$_{50}$. Even at this low DNA concentration, binding of DBD^{601} is accompanied by a large change in the anisotropy of the DNA, suggesting that in solution the signal is sensitive to formation of the higher-stoichiometry complexes. Indeed, even if we were to assume that the signal change now should report on the formation of a singly ligated species, the data cannot be fit with a simple 1:1 binding model (solid line). This strongly suggests that at low DNA concentrations the higher-stoichiometry complexes are not being detected by EMSAs and that their affinity must be higher than what would be inferred from the electrophoretic assays in Figure 1e.

Higher Concentrations of NaCl Abolish Binding of the Third DBD Molecule but Allow Formation of 2:1 DBD^{601}–DNA Complexes. The data presented in the previous sections were determined in the presence of a relatively low concentration of NaCl (50 mM) to amplify the presence of all possible bound states of DBD^{601}. Next, we explored the effect of increasing NaCl concentrations on the ability of DBD^{601} to access higher stoichiometries. The top panel of Figure 4a shows the change in fluorescence anisotropy of the TeloA substrate (labeled at the 3′-end of the top strand with FAM) as a function of the ratio of the total protein to DNA concentrations in buffer H with 50, 100, and 150 mM NaCl. It is evident that as the concentration of NaCl increases, there is a strong effect on the anisotropy corresponding to binding of the second and third DBD^{601} molecules. At the same time, binding of the first DBD^{601} molecule, as monitored by the initial phase of the anisotropy, is little affected by a 3-fold increase in NaCl concentration. Similar behavior is also observed when the relative total fluorescence intensity is monitored (Figure 4a, bottom panel). Increasing the NaCl concentration affects the binding of only the second and third DBD^{601} molecules (loss of the large fluorescence increase). Taken at face value, these data would suggest that higher salt concentrations inhibit formation of the higher-stoichiometry complexes. However, Figure 4b shows the change in the relative total fluorescence intensity for both TeloA and the lower-affinity HMRE, determined at 150 mM NaCl. At the same concentration of DNA for both substrates, DBD^{601} induces an initial quenching of the fluorophore followed by a

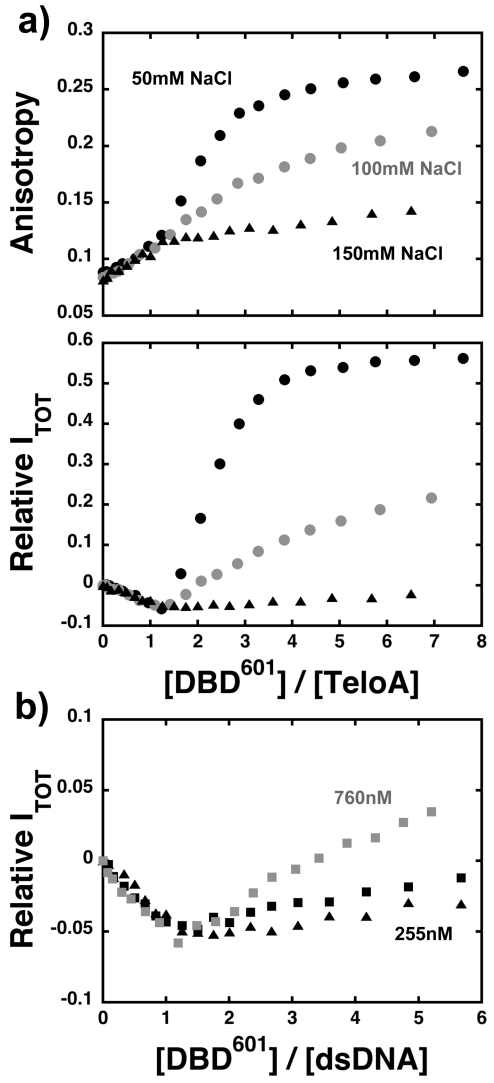

Figure 4. Higher salt concentration abolishes binding of the third DBD^{601} molecule. (a) Change in fluorescence anisotropy (top) and relative total intensity (bottom) as a function of DBD^{601}:DNA ratio for 255 nM TeloA FAM-labeled at the 3′-end of the top strand in buffer H at 50, 100, and 150 mM NaCl. (b) Change in relative total intensity as a function of DBD^{601}:DNA ratio in buffer HN$_{150}$ of 255 nM (black square) and 760 nM (gray square) HMRE FAM-labeled at the 3′-end of the top strand. The titration for 255 nM TeloA is shown as a reference (triangles).

small yet detectable fluorescence increase. This second phase of fluorescence enhancement becomes more evident when the concentration of HMRE is increased 3-fold, suggesting that this signal originates from a low-affinity binding phase. The simple observation of a change from quenching to an enhancement of the relative fluorescence intensity indicates that at least one additional molecule of DBD^{601} must bind even at this higher NaCl concentration. This conclusion is further reinforced by analytical equilibrium ultracentrifugation experiments with DBD^{601}–DNA complexes formed in buffer H at different NaCl concentrations (Table 2). While at 100 mM NaCl DBD^{601} is still able to access a stoichiometry of 3:1 on any of the substrates used, at 150 mM NaCl it is clear that only two molecules of DBD^{601} can bind at saturation. Interestingly, for the TeloA substrate, a 2:1 stoichiometry becomes more evident with a larger protein excess, suggesting that at this NaCl

dx.doi.org/10.1021/bi501049b | Biochemistry 2014, 53, 7471–7483

concentration it is more difficult to populate the doubly ligated species with this high-affinity Rap1 recognition sequence. Indeed, the doubly ligated species for the lower-affinity HMRE sequence is more easily detectable at a smaller excess of DBD^{601}. These data clearly show that higher NaCl concentrations prevent binding of a third DBD^{601} molecule but still allow for formation of at least a 2:1 complex even when a Rap1 recognition sequence is present in the substrate.

Isothermal Titration Calorimetry Shows Complex Behavior Consistent with More Than One Molecule of DBD^{601} Binding to a TeloA Substrate. The data in the previous sections clearly show that depending on the solution conditions, more than one molecule of DBD^{601} can bind to the model TeloA substrate. We also note that all the experiments presented thus far were performed in a way that enriches the population of the higher-stoichiometry complexes (e.g., increasing protein concentration). We have not yet found spectroscopic signal changes that would allow us to reliably monitor the interaction in the other direction (e.g., increasing DNA concentration to favor formation of the singly ligated species). However, for full-length Rap1, it has been shown that interaction with DNA can be monitored by isothermal titration calorimetry (ITC), at least in the direction that favors formation of a 1:1 complex (e.g., dsDNA as the titrant).[23,46] Therefore, we used ITC to study the binding of DBD^{601} to the TeloA substrate and performed titrations to access different end states in the reaction. Figure 5a shows the raw heats of injection for a selected direction (the reference titration is shown offset). Figure 5b shows the change in normalized heat as a function of molar ratio for titrations performed in either direction, DBD^{601} titrated into DNA (gray) or DNA titrated into DBD^{601} (black). It is clear that the titrations are not symmetric, as would be expected for a simple 1:1 interaction. Consistent with all the data presented in the previous sections, these data are indicative of a complex system in which different bound states can be achieved depending on the direction in which the experiment is performed. At a low molar ratio (i.e., excess protein to DNA) when TeloA is titrated into DBD^{601}, the reaction is accompanied by an initial phase with a large negative heat (approximately −40 kcal/mol). On the basis of the experiments presented so far, formation of a 3:1 complex of protein to DNA is expected to be favored in this concentration regime. Further increases in the total DNA concentration will then favor dissociation of the third DBD molecule and allow transition to lower-stoichiometry complexes. Indeed, the normalized heat decreases linearly to a ratio of ∼0.5 and then is followed by a steep drop in signal with a midpoint of ∼0.75 DNA/protein. In this direction of the titration, it would be expected that the reaction should reach a final stoichiometry of 1:1. It is, however, possible that the observed lower than expected midpoint of this second phase is affected by the large differences in affinity, and possibly the ΔH between the doubly and singly ligated species. The situation is very different when DBD^{601} is used as the titrant. In this direction, at a lower molar ratio (i.e., excess DNA to protein), formation of the singly ligated species is favored and likewise accompanied by an initial relatively constant ΔH value that is approximately half of that observed in the titrations performed in the opposite direction. The observed value in this direction (approximately −20 kcal/mol) provides an estimate of the ΔH for the singly ligated species. As the protein concentration increases, the molar heat decreases with a midpoint of ∼1.3 stoichiometry. Once again, this is a bit surprising on the basis of the data presented in the previous

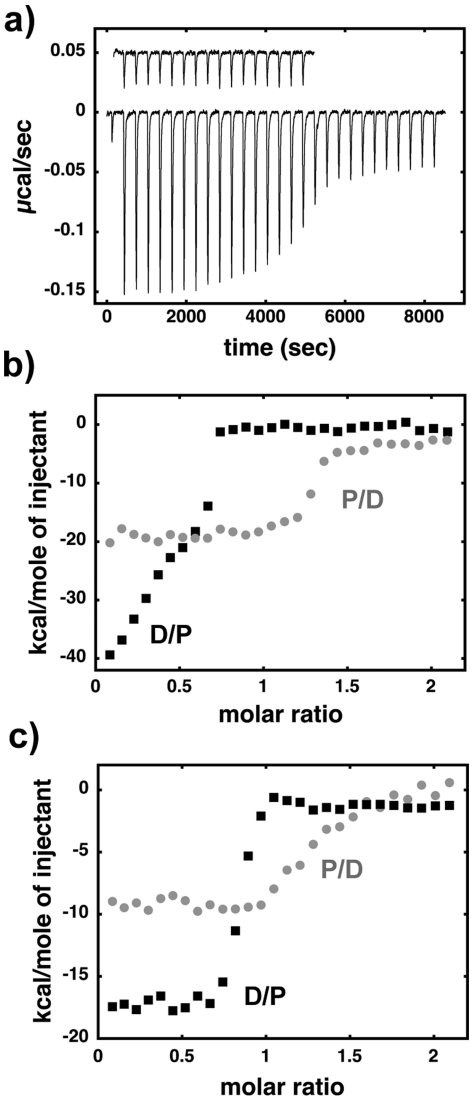

Figure 5. ITC shows a complex behavior consistent with formation of higher-order complexes, even at higher salt concentrations. (a) Raw heats of binding for a representative titration of DBD^{601} into TeloA in buffer HN_{50}. Also included (offset) is the contribution for the heat of dilution from a reference titration of DBD^{601}. (b) Change in normalized heat as a function of molar ratio for 20 μM TeloA titrated into 2 μM DBD^{601} (black) and 20 μM DBD^{601} titrated into 2 μM TeloA (gray) in buffer HN_{50} at 20 °C. (c) Change in normalized heat as a function of molar ratio for the same experiments as in panel b but performed in buffer HN_{150} at 20 °C.

sections, because in this direction of the titration the 3:1 protein−DNA complex should become enriched. The lower than expected stoichiometry suggests that formation of the high-affinity, singly ligated complex dominates the signal of the reaction, the net result being that any subsequent lower-affinity binding event remains undetectable under the conditions tested.

We showed that higher NaCl concentrations suppress binding of the third DBD^{601} molecule to DNA. Therefore, we next performed the same ITC experiments with TeloA in buffer HN_{150}. Figure 5c shows the isotherms obtained at this higher NaCl concentration with titrations performed in either direction. The asymmetry of the data obtained in both directions persists, again consistent with the data from fluorescence titrations and analytical equilibrium sedimentation

dx.doi.org/10.1021/bi501049b | Biochemistry 2014, 53, 7471−7483

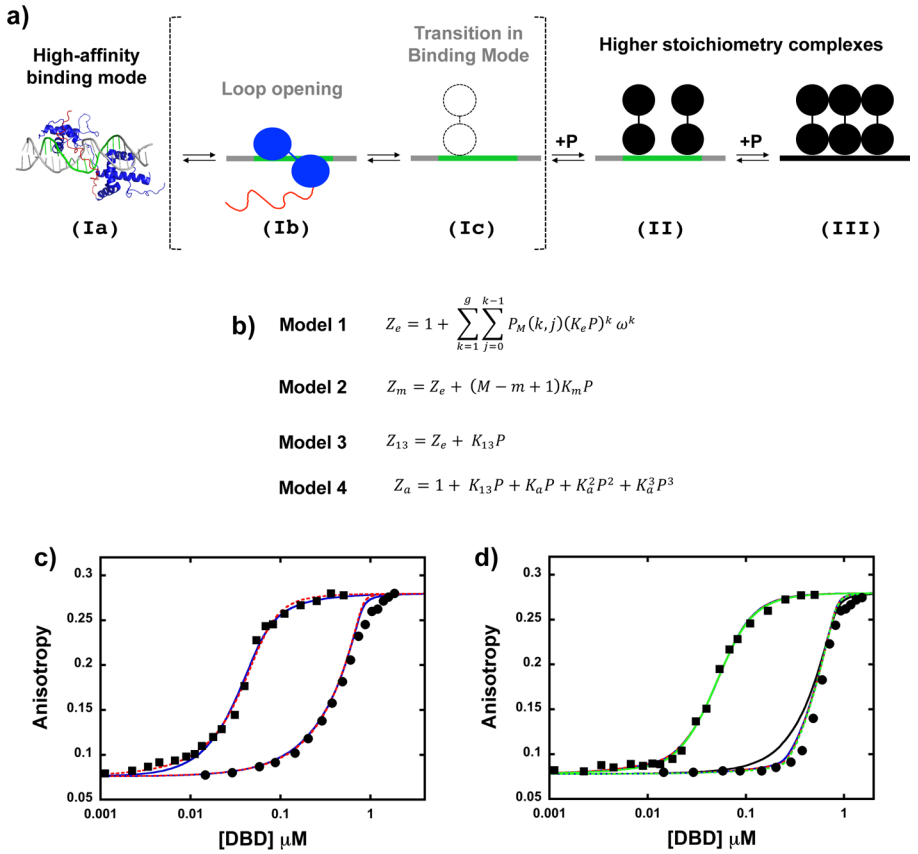

Figure 6. Rap1^{DBD} binds to dsDNA in multiple DNA binding modes. (a) Cartoon model of a possible pathway from the singly ligated complex (PDB entry 3UKG), bound in the high-affinity binding mode where both Myb domains interact with the recognition sequence, to the higher-stoichiometry complexes, where now only a single Myb domain binds to the dsDNA. (b) Partition functions that describe the different models used for analysis of the data. (c) Anisotropy binding data collected in buffer HN_{50} at 10 and 255 nM RND labeled at the 5′-end of the top strand. Blue lines are the fits with model 1 and red lines those with model 2. (d) Binding data as in panel c collected for TeloA. Black, blue, and red lines are the fits with model 3, and the green line is a fit with model 4. For details of the models, assumptions, and parameters, see the Supporting Information.

showing that even at 150 mM, DBD^{601} binds to TeloA with a stoichiometry of >1:1. At 150 mM NaCl when DNA is titrated into the protein, the initial decay phase observed at 50 mM is now abolished and the data show a constant initial value of approximately −17 kcal/mol with a midpoint of transition at ∼0.8. Moreover, at low molar ratios, the observed ΔH in this direction is higher than that determined by titrating DBD^{601} into DNA (approximately −17 vs −9 kcal/mol), suggesting there is an extra phase contributing to the signal. Once again, even at 150 mM NaCl when DBD^{601} is titrated into TeloA, the observed midpoint of transition is lower than would be expected for a 2:1 binding process. We also note that at 150 mM, the observed ΔH in this direction is approximately half of that determined at 50 mM, suggesting that increasing the NaCl concentration affects formation of the singly ligated complex. Initial attempts to fit the ITC data with simple models did not provide reliable estimates of the equilibrium constants and stoichiometries; therefore, we did not pursue further analysis and present the data as supporting evidence for the complex mode of interaction of DBD^{601} with the TeloA substrate.

DISCUSSION

In this work, we show a novel and unexpected DNA binding property of the DNA-binding domain of *S. cerevisiae* Rap1. Data from gel electrophoretic mobility shift assays, analytical ultracentrifugation, and equilibrium fluorescence titrations showed that in addition to forming a high-affinity 1:1 complex with its recognition sequence,[4,23,28,29,33,46,47] DBD^{601} can also form higher-stoichiometry complexes. Also, the ITC data show that different isotherms are observed depending on the direction of the experiment (i.e., DNA titrated into protein or vice versa), strongly suggesting that different end states can be populated and further supporting the conclusion that the system is more complex than a simple 1:1 system. These higher-stoichiometry complexes occur on dsDNA containing either telomeric (TeloA), ribosomal protein gene (RPG), silencer element (HMRE), or even random sequences. This indicates that binding of additional DBD^{601} molecules is not strictly sequence dependent, although the data suggest that it might be easier to populate the higher-stoichiometry complexes on random DNA sequences than on DNAs containing a Rap1 recognition sequence. Also, the data in Figure 3d show that these complexes can be formed at relatively low DNA concentrations, strongly suggesting that their affinity is higher than would be inferred by an EMSA.

Analytical sedimentation equilibrium experiments and fluorescence titrations show that at saturation three DBD^{601} molecules can bind to model dsDNA substrates. We also showed that in solution DBD^{601} behaves as a stable monomer at the highest protein concentrations used in these experiments (Figure 1c,d). Therefore, the observed higher stoichiometry is not due to the binding of higher-order oligomers of the protein present in solution. One possible way such a stoichiometry could be achieved is via a DNA-induced oligomerization of

dx.doi.org/10.1021/bi501049b | *Biochemistry* 2014, 53, 7471−7483

DBD^{601}.[44,48] If this were the case, we would expect formation of higher-order complexes to be favored on DNA substrates that bind DBD^{601} with higher affinity (i.e., containing the recognition sequence). Rather, the data show that a 3:1 complex is formed independent of the DNA substrate used and even better for one of random sequence, to which DBD^{601} binds weaker in the singly ligated state. Alternatively, on TeloA containing the Rap1 recognition sequence, the additional DBD molecules could bind to the 4 bp handles of the substrate. However, if the DBD were to bind nonspecifically to this region with such a small site size, then it would be expected that on the 21 bp dsDNA of random composition four or five molecules of DBD could bind at saturation. This is not the case. In addition, preliminary data with substrates containing varying lengths of the handle region strongly suggest that the second and third molecules of DBD^{601} do not bind to the handle regions (not shown). The question then becomes how many ways three DBD^{601} molecules can be arranged on a 21 bp dsDNA. The known Rap1 recognition sequence motif is at least 13 bp long.[3,28,30,31] The crystal structures of $Rap1^{DBD}$–DNA complexes show that the DNA-binding site is comprised of two half-sites of 5 bp that make contact with the two Myb-like domains, separated by a 3 bp linker.[23,28,29] However, in the high-stoichiometry complexes observed at the lower NaCl concentrations used in this work, the ability of three DBD^{601} molecules to bind the 21 bp substrates strongly suggests that 6–7 bp is sufficient for interaction. From the crystal structures, it is difficult to reconcile how such a short length of DNA would be bound by both Myb-like domains. Furthermore, work from the Negri lab showed that Rap1 can bind to just a single half-site, albeit with reduced affinity.[32] Our data suggest that in the transition from the singly to multiply ligated species, DBD^{601} switches modes of interaction, making contact with a different number of base pairs, from 13 to 6–7 bp. It should be pointed out that the salt dependence of DBD^{601}–DNA binding clearly shows that at 150 mM NaCl only a 2:1 complex can be significantly populated (Figure 4). Rather than a NaCl-dependent change in the apparent site size of the interaction (i.e., from 13 to ∼10 bp), we interpret the decreased stoichiometry at a higher salt concentration to be the result of a decreased affinity for the third DBD molecule.

We propose that the DNA-binding domain of Rap1 can bind dsDNA in at least two different binding modes. In one high-affinity mode, both Myb-like domains make contact with the entire recognition sequence, whereas in the other lower-affinity mode, only one of the two Myb-like domains binds DNA. Figure 6a shows a simple model for a dsDNA substrate containing a Rap1 recognition sequence depicting a possible pathway from the singly ligated complex to the higher-stoichiometry complexes. The most recent crystal structure of the DBD bound to a TeloA sequence shows that the ∼30 amino acids in the C-terminal region of the DBD (wrapping loop) fold back onto the N-terminal Myb-like domain to form a closed complex on DNA.[23] We propose that in solution, one possible path leading to the transition between the two binding modes is the transient opening of the C-terminal wrapping loop (Figure 6a, complex Ia-c). In the presence of excess protein, formation of complex Ic would then allow a second or third molecule of $Rap1^{DBD}$ to bind. At this stage, we do not know which one of the two Myb-like domains would be bound in complex Ic. The sequence conservation of the two half-sites in the Rap1 recognition motif and the crystal structures[29,49−51] suggest that the N-terminal Myb domain might be a possibility. On the basis of the model in Figure 6a, we analyzed the anisotropy binding data for the RND and TeloA substrates with different binding models (Figure 6b–d and Supporting Information). The estimated equilibrium dissociation constant of binding of DBD^{601} to the specific TeloA site in complex Ia (0.2–0.6 nM) is consistent with the reported value for this system[29] and is at least one order of magnitude lower than that for formation of complex Ic. It remains to be determined whether the transition from complex Ia to Ic is accompanied by and perhaps driven by cooperative binding of the second and third proteins in complexes II and III. At this stage, quantitative estimates of the equilibrium constants for complexes Ic–III are strongly dependent on the choice of model and assumptions and they will require additional information about the system (see the Supporting Information).

The data presented in this work show that the transition between binding modes occurs even on substrates containing a Rap1 recognition sequence and at a DNA concentration as low as 10 nM. This suggests that these alternative binding modes can coexist with the high-affinity mode at protein concentrations lower than those needed to fully populate them. It remains to be determined whether under normal expression conditions the Rap1 concentration *in vivo* is enough to support the transition between binding modes, even though Rap1 is a highly abundant protein.[52] Interestingly, work from the Shore lab showed that overexpression of Rap1 has a toxic phenotype leading to growth inhibition and that the presence of an intact DNA-binding domain is required for toxicity.[25] Under these conditions, it is possible that $Rap1^{DBD}$ can access higher stoichiometries (i.e., switch binding modes) even on the high-affinity Rap1 recognition sequences. We speculate that our observation that the DBD can switch between binding modes as a function of protein concentration might, at least in part, provide a basis for the toxicity of full-length protein overexpression, especially at Rap1-binding sites involved in transcriptional regulation and repression.

The situation is different, however, on the dsDNA substrate of random sequence composition. We showed that for the RND substrate in the singly ligated complex, the anisotropy and fluorescence intensity have different signatures compared to that of TeloA, RPG, or HMRE (Figure 3). We interpret these differences in signal response as an indication that the 1:1 DBD^{601}–DNA complexes are in different conformations. This interpretation is further supported by the observed differences in both the sedimentation coefficient and the electrophoretic mobility of the 1:1 complex formed on the RND substrate (Figure 2). For a DNA of random sequence composition, we propose that if complex Ia in Figure 6a forms, the lack of a proper, high-affinity recognition sequence for the two Myb-like domains does not allow for a stable closure of the C-terminal wrapping loop. Therefore, on a random DNA sequence, $Rap1^{DBD}$ would be more prone to transition to the second binding mode (complex Ic). This is also supported by analysis of the data in Figure 6c where model 1, which does not include formation of complex Ia, is sufficient to fit the data. Interestingly, in addition to telomeric sites, Rap1 can be chromatin immunoprecipitated even at distances from the distal telomeric ends of 2–4 kbp.[53] At these sites, Rap1 must bind through nonspecific DNA interactions, and it has been suggested that this nonspecific DNA binding could be a means to allow spreading of Rap1 from telomeric ends.[53] It is intriguing to speculate that if Rap1 binds to these nonspecific sites and spreads, it might do so using the alternative, lower-

affinity binding mode (i.e., single Myb bound in complex Ic). Also, the analysis in Figure 6c with model 1 (see the Supporting Information) suggests the presence of positive cooperative interactions in complex II. This would lead to stabilization of a Rap1 complex even on DNAs of random composition for which the affinity of the DBD [~1 μM (see the Supporting Information)] is much lower than for its recognition sequence. Moreover, in this alternative binding mode (complexes Ic–III), the bound Rap1^{DBD} would be very different from the one at telomeres, where both Myb-like domains are expected to interact with high affinity.[23,28,29] This might impact the interaction of Rap1 with its interacting proteins (e.g., Rif1, Rif2, Sir3, and Sir4)[14,15,18,53] at telomeres versus nontelomeric sites and/or help establish the boundary between telomeric and nontelomeric regions.

In summary, we showed that the DNA-binding domain of Rap1 can bind to DNA with stoichiometries higher than previously anticipated, and we propose that this can be achieved via its ability to transition between two different DNA binding modes. The transition between binding modes has been documented for *E. coli* SSB,[54−56] HU,[57−60] human and yeast RPA,[39,61,62] and mammalian DNA Pol β.[63,64] It is clear that in the different binding modes these proteins form complexes with different properties. The ability of these systems to bind DNA with different binding modes is proposed to affect their function *in vivo*.[65] We currently do not know the functional role *in vivo* of the presence of different binding modes for the Rap1 DNA-binding domain. Also, the DBD comprises only approximately one-third of the full-length protein molecule. It remains to be determined how this novel DNA binding property is affected in the context of the full-length protein, where the DBD might not bind to DNA as a truly independent domain. The findings in this work suggest that the ability of the DBD to access different binding modes may be a possible point of regulation. The highly modular domain organization of Rap1 and the observation that different regions participate in different functions of the protein (see the introductory section) suggest the possibility that the transition between binding modes could be regulated either internally by its other domains or externally through interactions with Rap1 interaction factors.

■ ASSOCIATED CONTENT

Supporting Information

Description and assumptions of the models in Figure 6b used to fit the data in panels c and d. This material is available free of charge via the Internet at http://pubs.acs.org.

■ AUTHOR INFORMATION

Corresponding Author

*Department of Biochemistry and Molecular Biophysics, Washington University School of Medicine, 660 S. Euclid Ave., Box 8231, St. Louis, MO 63110. E-mail: galletto@biochem.wustl.edu. Phone: (314) 362-4368. Fax: (314) 362-7183.

Present Address

†E.A.F.: Department of Molecular and Structural Biochemistry, North Carolina State University, 128 Polk Hall, Campus Box 7622, Raleigh, NC 27695.

Funding

This work was supported by a grant from the National Institutes of Health (GM098509 to R.G.).

Notes

The authors declare no competing financial interest.

■ ACKNOWLEDGMENTS

We thank Prof. T. M. Lohman and Dr. A. Kozlov for the extensive use of the isothermal titration calorimeter and helpful comments. We thank Prof. T. Heyduk for help with lifetime and rotational correlation time measurements. We thank Prof. P. M. Burgers for access to reagents.

■ ABBREVIATIONS

dsDNA, double-stranded DNA; DBD, DNA-binding domain; EMSA, electrophoretic mobility shift assay; AUC, analytical ultracentrifugation; ITC, isothermal titration calorimetry.

■ REFERENCES

(1) Shore, D., and Nasmyth, K. (1987) Purification and cloning of a DNA binding protein from yeast that binds to both silencer and activator elements. *Cell 51*, 721–732.

(2) Kurtz, S., and Shore, D. (1991) RAP1 protein activates and silences transcription of mating-type genes in yeast. *Genes Dev. 5*, 616–628.

(3) Lieb, J. D., Liu, X., Botstein, D., and Brown, P. O. (2001) Promoter-specific binding of Rap1 revealed by genome-wide maps of protein-DNA association. *Nat. Genet. 28*, 327–334.

(4) Garbett, K. A., Tripathi, M. K., Cencki, B., Layer, J. H., and Weil, P. A. (2007) Yeast TFIID serves as a coactivator for Rap1p by direct protein-protein interaction. *Mol. Cell. Biol. 27*, 297–311.

(5) Layer, J. H., Miller, S. G., and Weil, P. A. (2010) Direct Transactivator-Transcription Factor IID (TFIID) Contacts Drive Yeast Ribosomal Protein Gene Transcription. *J. Biol. Chem. 285*, 15489–15499.

(6) Layer, J. H., and Weil, P. A. (2013) Direct TFIIA-TFIID Protein Contacts Drive Budding Yeast Ribosomal Protein Gene Transcription. *J. Biol. Chem. 288*, 23273–23294.

(7) Warner, J. R. (1999) The economics of ribosome biosynthesis in yeast. *Trends Biochem. Sci. 24*, 437–440.

(8) Lascaris, R. F., Mager, W. H., and Planta, R. J. (1999) DNA-binding requirements of the yeast protein Rap1p as selected in silico from ribosomal protein gene promoter sequences. *Bioinformatics 15*, 267–277.

(9) Lee, T. I., Rinaldi, N. J., Robert, F., Odom, D. T., Bar-Joseph, Z., Gerber, G. K., Hannett, N. M., Harbison, C. T., Thompson, C. M., Simon, I., Zeitlinger, J., Jennings, E. G., Murray, H. L., Gordon, D. B., Ren, B., Wyrick, J. J., Tagne, J. B., Volkert, T. L., Fraenkel, E., Gifford, D. K., and Young, R. A. (2002) Transcriptional regulatory networks in *Saccharomyces cerevisiae*. *Science 298*, 799–804.

(10) Schawalder, S. B., Kabani, M., Howald, I., Choudhury, U., Werner, M., and Shore, D. (2004) Growth-regulated recruitment of the essential yeast ribosomal protein gene activator Ifh1. *Nature 432*, 1058–1061.

(11) Menon, B. B., Sarma, N. J., Pasula, S., Deminoff, S. J., Willis, K. A., Barbara, K. E., Andrews, B., and Santangelo, G. M. (2005) Reverse recruitment: The Nup84 nuclear pore subcomplex mediates Rap1/Gcr1/Gcr2 transcriptional activation. *Proc. Natl. Acad. Sci. U.S.A. 102*, 5749–5754.

(12) Wellinger, R. J., and Zakian, V. A. (2012) Everything you ever wanted to know about *Saccharomyces cerevisiae* telomeres: Beginning to end. *Genetics 191*, 1073–1105.

(13) Longtine, M. S., Wilson, N. M., Petracek, M. E., and Berman, J. (1989) A yeast telomere binding activity binds to two related telomere sequence motifs and is indistinguishable from RAP1. *Curr. Genet. 16*, 225–239.

(14) Hardy, C. F., Sussel, L., and Shore, D. (1992) A RAP1-interacting protein involved in transcriptional silencing and telomere length regulation. *Genes Dev. 6*, 801–814.

(15) Wotton, D., and Shore, D. (1997) A novel Rap1p-interacting factor, Rif2p, cooperates with Rif1p to regulate telomere length in *Saccharomyces cerevisiae*. *Genes Dev. 11*, 748−760.
(16) Marcand, S., Gilson, E., and Shore, D. (1997) A protein-counting mechanism for telomere length regulation in yeast. *Science 275*, 986−990.
(17) Levy, D. L., and Blackburn, E. H. (2004) Counting of Rif1p and Rif2p on *Saccharomyces cerevisiae* telomeres regulates telomere length. *Mol. Cell. Biol. 24*, 10857−10867.
(18) Moretti, P., Freeman, K., Coodly, L., and Shore, D. (1994) Evidence that a complex of SIR proteins interacts with the silencer and telomere-binding protein RAP1. *Genes Dev. 8*, 2257−2269.
(19) Palladino, F., Laroche, T., Gilson, E., Axelrod, A., Pillus, L., and Gasser, S. M. (1993) Sir3 and Sir4 Proteins Are Required for the Positioning and Integrity of Yeast Telomeres. *Cell 75*, 543−555.
(20) Hecht, A., Laroche, T., Strahlbolsinger, S., Gasser, S. M., and Grunstein, M. (1995) Histone H3 and H4 N-Termini Interact with Sir3 and Sir4 Proteins: A Molecular-Model for the Formation of Heterochromatin in Yeast. *Cell 80*, 583−592.
(21) Morse, R. H. (2000) RAP, RAP, open up! New wrinkles for RAP1 in yeast. *Trends Genet. 16*, 51−53.
(22) Shore, D. (1994) RAP1: A protean regulator in yeast. *Trends Genet. 10*, 408−412.
(23) Matot, B., Le Bihan, Y. V., Lescasse, R., Pérez, J., Miron, S., David, G., Castaing, B., Weber, P., Raynal, B., Zinn-Justin, S., Gasparini, S., and Le Du, M. H. (2012) The orientation of the C-terminal domain of the *Saccharomyces cerevisiae* Rap1 protein is determined by its binding to DNA. *Nucleic Acids Res. 40*, 3197−3207.
(24) Mizuno, T., Kishimoto, T., Shinzato, T., Haw, R., Chambers, A., Wood, J., Sinclair, D., and Uemura, H. (2004) Role of the N-terminal region of RapIp in the transcriptional activation of glycolytic genes in *Saccharomyces cerevisiae*. *Yeast 21*, 851−866.
(25) Freeman, K., Gwadz, M., and Shore, D. (1995) Molecular and Genetic-Analysis of the Toxic Effect of Rap1 Overexpression in Yeast. *Genetics 141*, 1253−1262.
(26) Kyrion, G., Boakye, K. A., and Lustig, A. J. (1992) C-Terminal Truncation of Rap1 Results in the Deregulation of Telomere Size, Stability, and Function in *Saccharomyces cerevisiae*. *Mol. Cell. Biol. 12*, 5159−5173.
(27) Hardy, C. F. J., Balderes, D., and Shore, D. (1992) Dissection of a Carboxy-Terminal Region of the Yeast Regulatory Protein Rap1 with Effects on Both Transcriptional Activation and Silencing. *Mol. Cell. Biol. 12*, 1209−1217.
(28) Konig, P., Giraldo, R., Chapman, L., and Rhodes, D. (1996) The crystal structure of the DNA-binding domain of yeast RAP1 in complex with telomeric DNA. *Cell 85*, 125−136.
(29) Taylor, H. O., O'Reilly, M., Leslie, A. G., and Rhodes, D. (2000) How the multifunctional yeast Rap1p discriminates between DNA target sites: A crystallographic analysis. *J. Mol. Biol. 303*, 693−707.
(30) Conrad, M. N., Wright, J. H., Wolf, A. J., and Zakian, V. A. (1990) RAP1 protein interacts with yeast telomeres in vivo: Overproduction alters telomere structure and decreases chromosome stability. *Cell 63*, 739−750.
(31) Graham, I. R., and Chambers, A. (1994) Use of a selection technique to identify the diversity of binding sites for the yeast RAP1 transcription factor. *Nucleic Acids Res. 22*, 124−130.
(32) Del Vescovo, V., De Sanctis, V., Bianchi, A., Shore, D., Di Mauro, E., and Negri, R. (2004) Distinct DNA elements contribute to Rap1p affinity for its binding sites. *J. Mol. Biol. 338*, 877−893.
(33) Williams, T. L., Levy, D. L., Maki-Yonekura, S., Yonekura, K., and Blackburn, E. H. (2010) Characterization of the yeast telomere nucleoprotein core: Rap1 binds independently to each recognition site. *J. Biol. Chem. 285*, 35814−35824.
(34) Schuck, P. (2003) On the analysis of protein self-association by sedimentation velocity analytical ultracentrifugation. *Anal. Biochem. 320*, 104−124.
(35) Balbo, A., Brown, P. H., Braswell, E. H., and Schuck, P. (2007) Measuring protein-protein interactions by equilibrium sedimentation. In *Current Protocols in Immunology*, Chapter 18, Unit 18, 18, Wiley, New York.
(36) Schuck, P. (1998) Sedimentation analysis of noninteracting and self-associating solutes using numerical solutions to the Lamm equation. *Biophys. J. 75*, 1503−1512.
(37) Dam, J., Velikovsky, C. A., Mariuzza, R. A., Urbanke, C., and Schuck, P. (2005) Sedimentation velocity analysis of heterogeneous protein-protein interactions: Lamm equation modeling and sedimentation coefficient distributions c(s). *Biophys. J. 89*, 619−634.
(38) Hayes, D., Laue, T., and Philo, J. (1995) *Program Sednterp: sedimentation interpretation program*, University of New Hampshire, Durham, NH.
(39) Kumaran, S., Kozlov, A. G., and Lohman, T. M. (2006) *Saccharomyces cerevisiae* replication protein A binds to single-stranded DNA in multiple salt-dependent modes. *Biochemistry 45*, 11958−11973.
(40) Lakowicz, J. R. (1999) *Principles of Fluorescence Spectroscopy*, Plenum Press, New York.
(41) Kozlov, A. G., Galletto, R., and Lohman, T. M. (2012) SSB-DNA binding monitored by fluorescence intensity and anisotropy. *Methods Mol. Biol. 922*, 55−83.
(42) Giraldo, R., and Rhodes, D. (1994) The yeast telomere-binding protein RAP1 binds to and promotes the formation of DNA quadruplexes in telomeric DNA. *EMBO J. 13*, 2411−2420.
(43) Eftink, M. R. (1997) Fluorescence methods for studying equilibrium macromolecule-ligand interactions. *Methods Enzymol. 278*, 221−257.
(44) Barranco-Medina, S., and Galletto, R. (2010) DNA binding induces dimerization of *Saccharomyces cerevisiae* Pif1. *Biochemistry 49*, 8445−8454.
(45) Sjoback, R., Nygren, J., and Kubista, M. (1995) Absorption and Fluorescence Properties of Fluorescein. *Spectrochim. Acta, Part A 51*, L7−L21.
(46) Le Bihan, Y. V., Matot, B., Pietrement, O., Giraud-Panis, M. J., Gasparini, S., Le Cam, E., Gilson, E., Sclavi, B., Miron, S., and Le Du, M. H. (2013) Effect of Rap1 binding on DNA distortion and potassium permanganate hypersensitivity. *Acta Crystallogr. D69*, 409−419.
(47) Blackburn, E. H. (2000) Telomere states and cell fates. *Nature 408*, 53−56.
(48) Wong, I., Chao, K. L., Bujalowski, W., and Lohman, T. M. (1992) DNA-induced dimerization of the *Escherichia coli* rep helicase. Allosteric effects of single-stranded and duplex DNA. *J. Biol. Chem. 267*, 7596−7610.
(49) Vignais, M. L., Huet, J., Buhler, J. M., and Sentenac, A. (1990) Contacts between the Factor Tuf and Rpg Sequences. *J. Biol. Chem. 265*, 14669−14674.
(50) Idrissi, F. Z., Fernandez-Larrea, J. B., and Pina, B. (1998) Structural and functional heterogeneity of Rap1p complexes with telomeric and UASrpg-like DNA sequences. *J. Mol. Biol. 284*, 925−935.
(51) Idrissi, F. Z., and Pina, B. (1999) Functional divergence between the half-sites of the DNA-binding sequence for the yeast transcriptional regulator Rap1p. *Biochem. J. 341*, 477−482.
(52) Buchman, A. R., Kimmerly, W. J., Rine, J., and Kornberg, R. D. (1988) Two DNA-binding factors recognize specific sequences at silencers, upstream activating sequences, autonomously replicating sequences, and telomeres in *Saccharomyces cerevisiae*. *Mol. Cell. Biol. 8*, 210−225.
(53) Moretti, P., and Shore, D. (2001) Multiple interactions in sir protein recruitment by Rap1p at silencers and telomeres in yeast. *Mol. Cell. Biol. 21*, 8082−8094.
(54) Lohman, T. M., and Overman, L. B. (1985) Two binding modes in *Escherichia coli* single strand binding protein-single stranded DNA complexes. Modulation by NaCl concentration. *J. Biol. Chem. 260*, 3594−3603.
(55) Bujalowski, W., and Lohman, T. M. (1986) *Escherichia coli* Single-Strand Binding-Protein Forms Multiple, Distinct Complexes with Single-Stranded-DNA. *Biochemistry 25*, 7799−7802.

(56) Griffith, J. D., Harris, L. D., and Register, J. (1984) Visualization of Ssb-Ssdna Complexes Active in the Assembly of Stable Reca-DNA Filaments. *Cold Spring Harbor Symp. Quant. Biol. 49*, 553−559.
(57) Koh, J., Saecker, R. M., and Record, M. T. (2008) DNA Binding Mode Transitions of *Escherichia coli* HU alpha beta: Evidence for Formation of a Bent DNA-Protein Complex on Intact, Linear Duplex DNA. *J. Mol. Biol. 383*, 324−346.
(58) Koh, J., Shkel, I., Saecker, R. M., and Record, M. T. (2011) Nonspecific DNA Binding and Bending by HU alpha beta: Interfaces of the Three Binding Modes Characterized by Salt-Dependent Thermodynamics. *J. Mol. Biol. 410*, 241−267.
(59) van Noort, J., Verbrugge, S., Goosen, N., Dekker, C., and Dame, R. T. (2004) Dual architectural roles of HU: Formation of flexible hinges and rigid filaments. *Proc. Natl. Acad. Sci. U.S.A. 101*, 6969−6974.
(60) Xiao, B. T., Johnson, R. C., and Marko, J. F. (2010) Modulation of HU-DNA interactions by salt concentration and applied force. *Nucleic Acids Res. 38*, 6176−6185.
(61) Blackwell, L. J., and Borowiec, J. A. (1994) Human Replication Protein-a Binds Single-Stranded-DNA in 2 Distinct Complexes. *Mol. Cell. Biol. 14*, 3993−4001.
(62) Blackwell, L. J., Borowiec, J. A., and Mastrangelo, I. A. (1996) Single-stranded-DNA binding alters human replication protein a structure and facilitates interaction with DNA-dependent protein kinase. *Mol. Cell. Biol. 16*, 4798−4807.
(63) Jezewska, M. J., Rajendran, S., and Bujalowski, W. (1998) Transition between different binding modes in rat DNA polymerase β-ssDNA complexes. *J. Mol. Biol. 284*, 1113−1131.
(64) Rajendran, S., Jezewska, M. J., and Bujalowski, W. (1998) Human DNA polymerase β recognizes single-stranded DNA using two different binding modes. *J. Biol. Chem. 273*, 31021−31031.
(65) Lohman, T. M., and Ferrari, M. E. (1994) *Escherichia coli* Single-Stranded DNA-Binding Protein: Multiple DNA-Binding Modes and Cooperativities. *Annu. Rev. Biochem. 63*, 527−570.